Molybdenum-Driven Electronic Restructuring of Iron Carbides Unlocks Faster Volmer Kinetics in Alkaline Hydrogen Evolution

Animesh Khaund[a,b], Srijib Das[b,c], Esin Aydemir[d], Saptarshi Ghosh Dastider[e], Srija Ghosh[a], Aniruddha Kundu[e], Tapas Kuila[b,c], Koushik Barman[a]*, Brian M Tackett[d]*, Kingshuk Roy[a,b]*

[a] Research Institute for Sustainable Energy, TCG Centres for Research and Education in Science and Technology, Salt Lake, Kolkata 700091, West Bengal, India
[b] Academy of Scientific and Innovative Research (AcSIR), Ghaziabad 201002, India
[c] Electric Mobility & Tribology Research Group, CSIR- Central Mechanical Engineering Research Institute, Durgapur 713209, India
[d] Davidson School of Chemical Engineering, Purdue University, West Lafayette, IN 47907, USA
[e] Department of Chemistry, Indian Institute of Space Science and Technology, Valiamala PO, Thiruvananthapuram - 695547, India
[f] Centre for Interdisciplinary Research, SRM University-AP, Amaravati, Andhra Pradesh 522240, India

Instrumentation and Methods

All electrochemical experiments were carried out using CHI bipotentiostat with three electrode setup. Glassy carbon electrode/ ITO used as working electrode, carbon rod as counter, and Ag/AgCl (0.1 M KCl) as reference electrode. Potential was converted to RHE according to the Nernst equation

$E_{RHE} = E_{Ag/AgCl} + 0.059\ pH + Eo_{\ Ag/AgCl}$, $Eo_{\ Ag/AgCl} = 0.1976$ at 25 °C

Details of H2 calibration and calculation of Faradaic efficiency

Internal calibration of ECMS (Spectro Inlets) m/z=2 signal for hydrogen production was carried out with a polycrystalline platinum disk electrode in 1M $HClO_4$ electrolyte. Reductive chronopotentiometry (CP) measurements were taken subsequently at -30 µA, -25 µA, -2 µA 0, -15 µA, and -10 µA for 300 seconds to ensure steady-state detector current in MS spectrum. Each CP step was followed by and OCV step for 300 seconds. Assuming 100% Faradaic efficiency for H2 formation, m/z=2 peaks at each CP step were integrated and plotted against the theoretical amount of H_2 formed based on Faraday's Law. A linear line fit to the calibration curve yielded a calibration factor of 0.44 C/mol.

The raw signal current in MS spectrum was converted to H2 flux by the calibration factor obtained via internal H2 calibration. The area under m/z=2 signal was integrated over the interval of reductive chronoamperometry (CA) step and divided by 0.44 C/mol to obtain the moles of H2 produced:

$$n_{H2} = \frac{\int_0^t I_{detector} dt}{0.44 C/mol}$$

The amount of charge spent for H2 formation was calculated via Faraday's Law:

$q_{H2} = 2Fn_{H2}$

Where F stands for Faraday constant (F = 96485 C/mol e^-).

Faradaic efficiency was calculated by dividing the amount of charge spent for H2 formation by the total amount of charge generated during the CA step:

$$Faradaic\ efficiency\ (\%) = \frac{q_{H2}}{q_{total}}\ x\ 100$$

The total amount of charge (q_{total}) generated during CA steps was calculated by integrating the current-time response over the duration of the potential hold, using the zero current baseline as a reference.

ECMS Procedure

ECMS experiments were performed with helium (research purity 6N, A-OX Welding) as the carrier gas, supplied through an internal mass flow controller, providing a convective flow of volatile and gaseous species to mass spectrometer. A glassy carbon (GC) disk working electrode of 5mm diameter (Pine Research Instrumentation), Ag/AgCl reference electrode (3.4M KCl), and Pt counter electrode were connected to a potentiostat (Biologic SP-300). EC-Lab and Zilien software (Spectro Inlets) were used for electrochemical and MS data collection, respectively.

Calculation of Turn Over Frequency (TOF)

Supposing that all the active sites were accessible to the electrolyte, TOF values can be calculated by the following equations

$$\mathrm{TOF} = \frac{1}{2}\frac{I}{n\mathrm{F}}$$

where the I, n, and F are corresponding to the current density (in A cm^{-2}), the number of active sites (mol cm^{-2}), and Faraday constant (~ 96484 C mol^{-1}) during the LSV measurements in 0.1 M KOH, respectively.

TOF = ~0.16 s^{-1}

Mass Activity (η= 250 mV)

Commercial 20% Pt/C = 525 mA mg^{-1}_{Pt}

FeMo-NC2 = 495 mA mg^{-1}_{Metal}

Calculation of ECSA

ECSA can be calculated by using the following equation

$$\mathrm{ECSA} = \frac{C_{dl}}{C_s}$$

Where C_{dl} Double layer capacitance (mF), C_s specific capacitance (mF cm^{-2}). For the calculation and comparison of ECSA, a C_s value of 0.040 mF cm^{-2} was used, as reported in prior literature and summarized in **Table S12**.

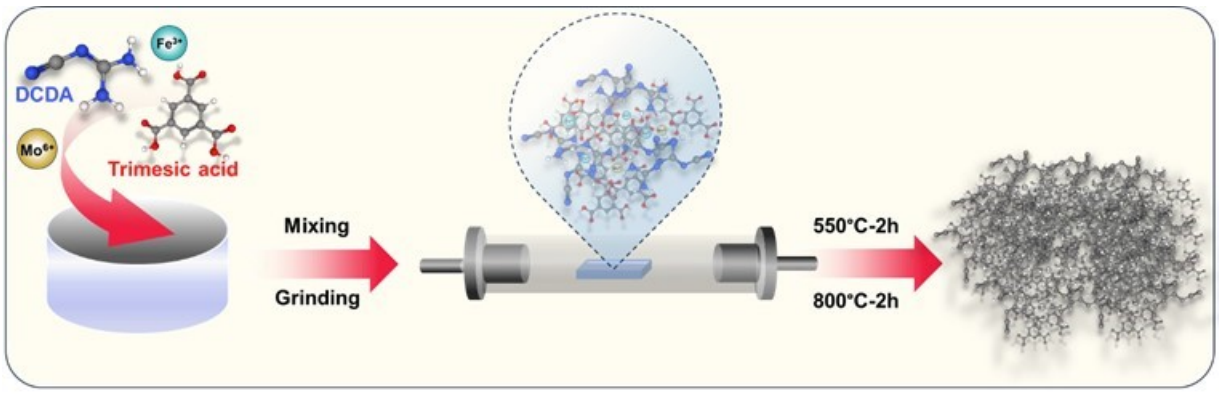

Figure S1: Schematic illustration of the Synthesis procedure for FeMo-NC based catalysts.

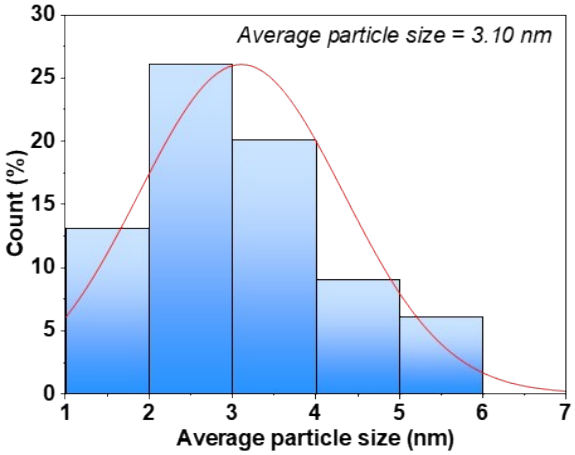

Figure S2: Particle size distribution.

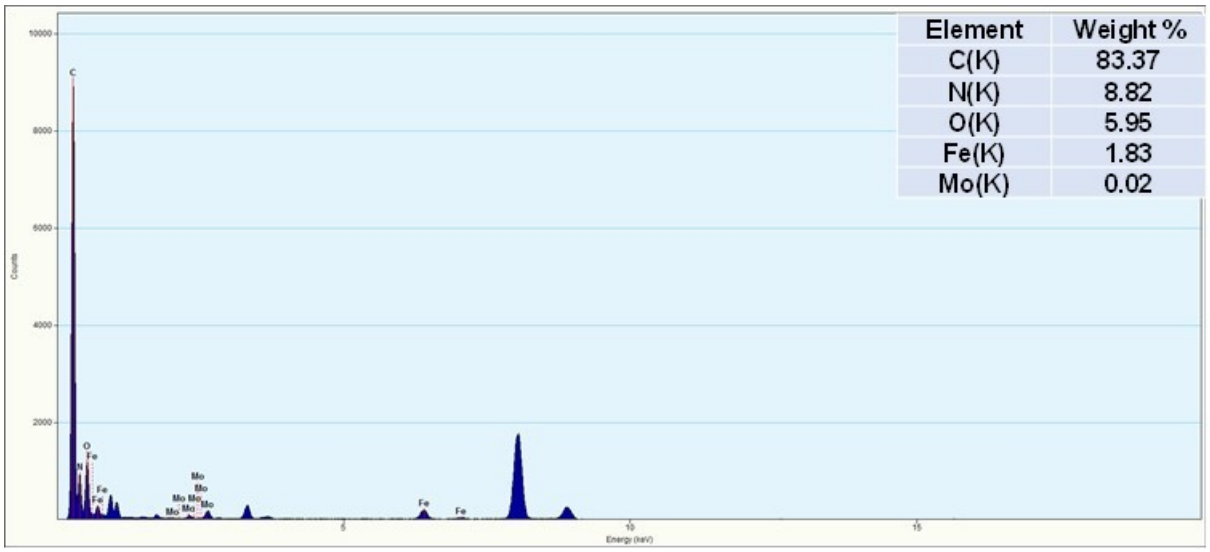

Figure S3: EDX mapping of FeMo-NC2

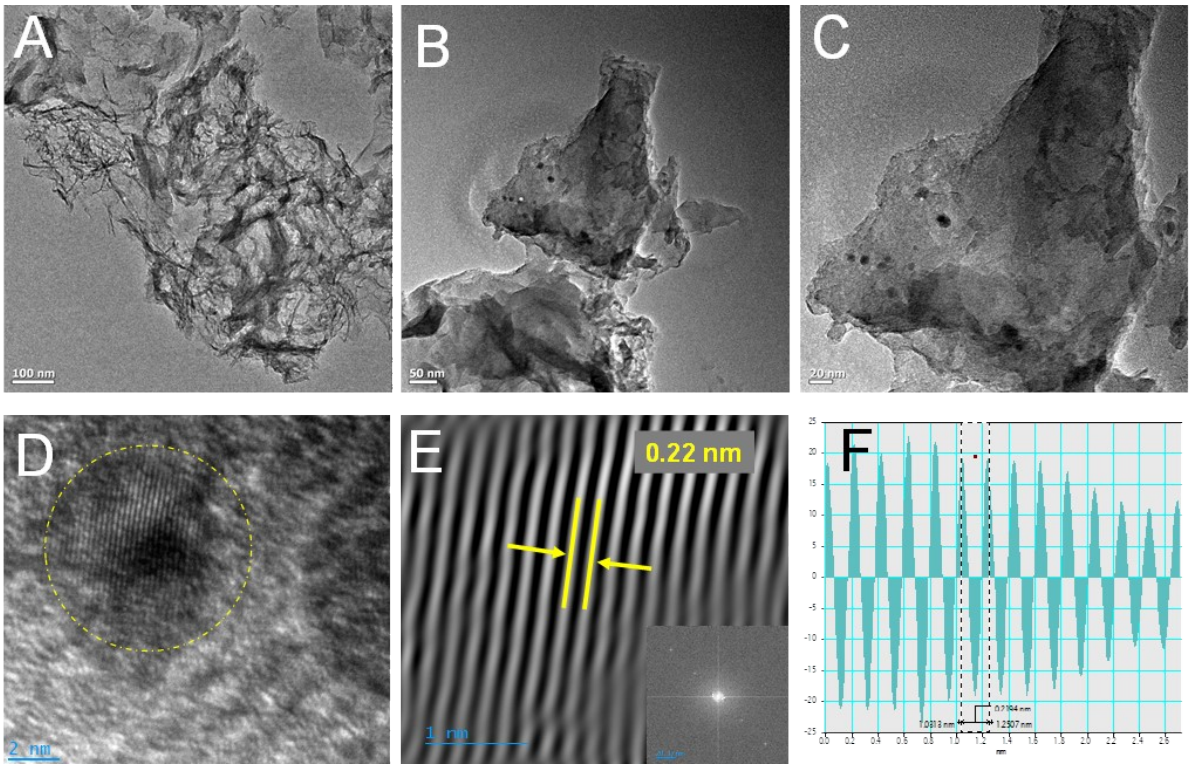

Figure S4: (**A-C**) TEM image of Fe-NC at different magnifications, (**D**) HRTEM image, (**E**) corresponding IFFT Pattern and (**F**) line spectrum.

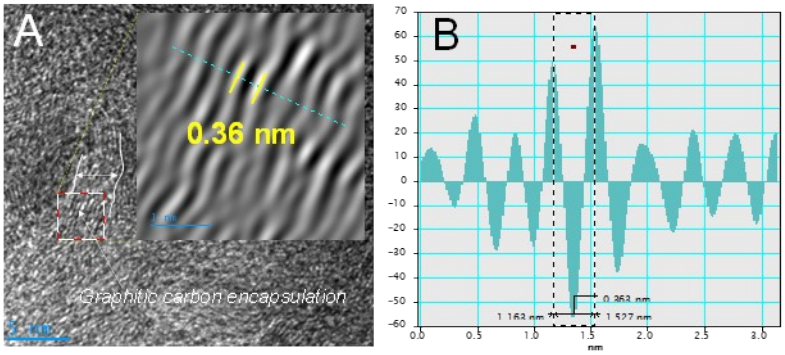

Figure S5: (**A**)HRTEM image of the Fe-NC catalysts (inset: IFFT pattern showing the d-spacing), and (**B**) corresponding line spectrum.

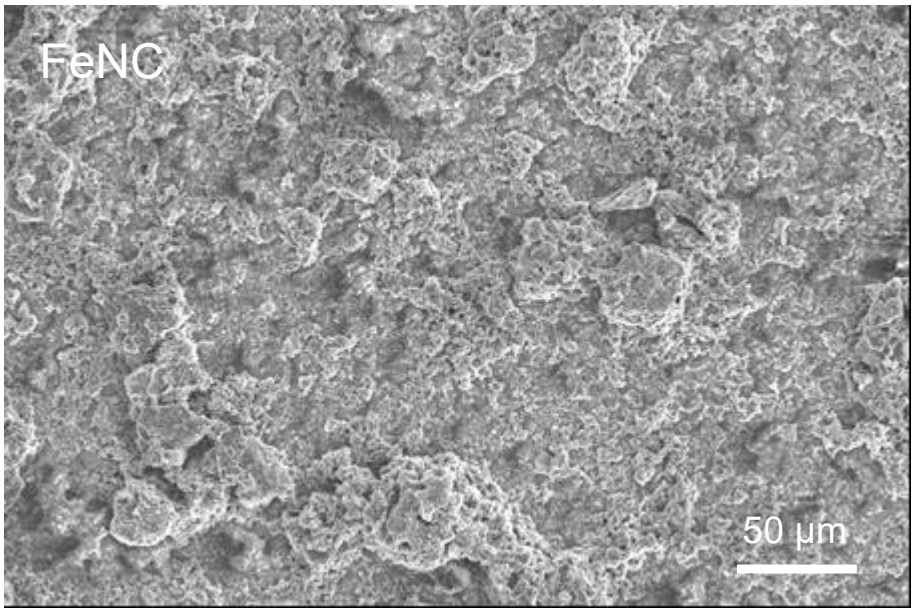

Figure S6: SEM image of FeNC.

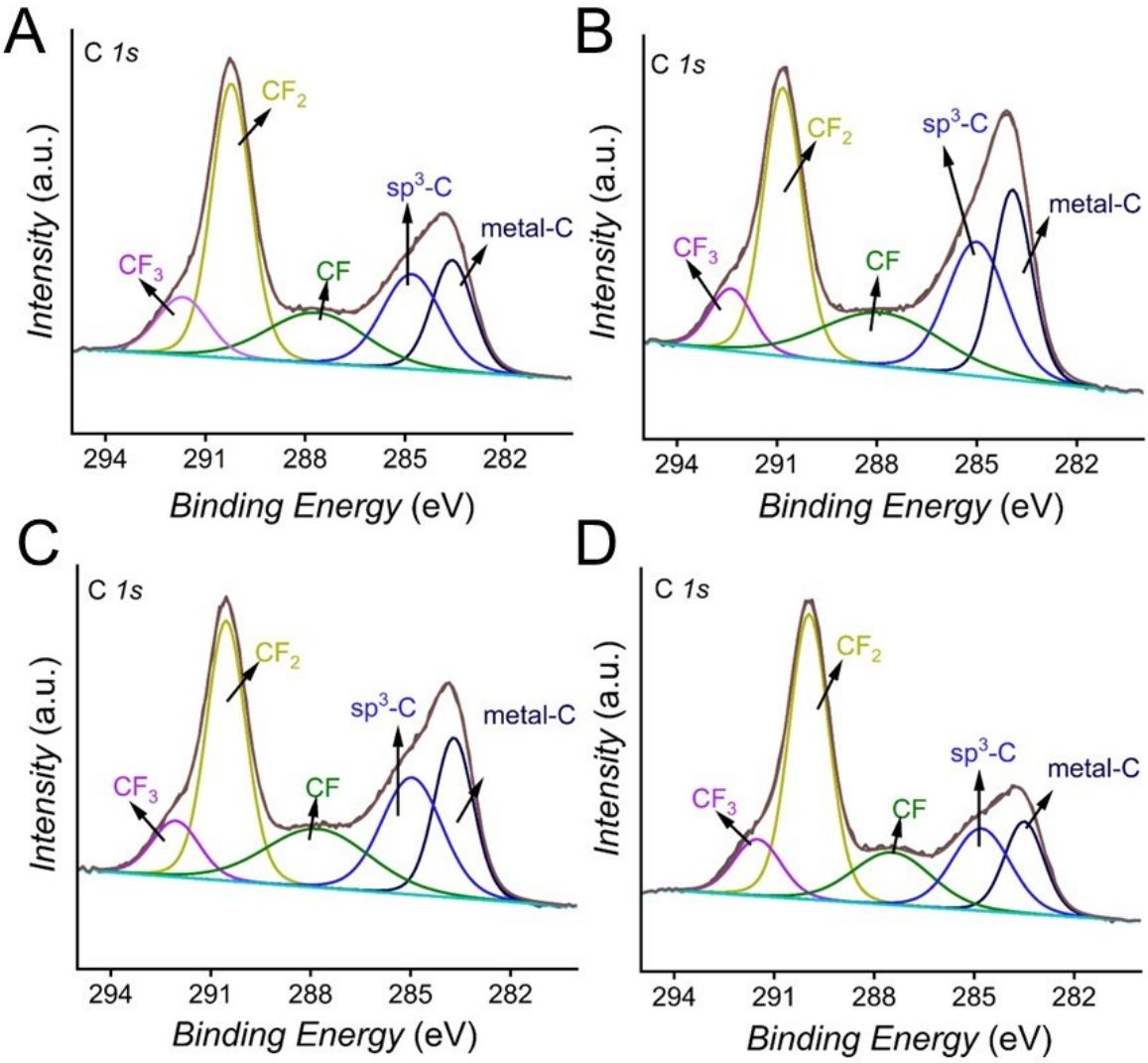

Figure S7: C *1s* XPS data of **(A)** FeMo-NC1, **(B)** FeMo-NC2, (**C**) FeMo-NC3 and **(D)** FeNC; containing nafion on ITO.

.

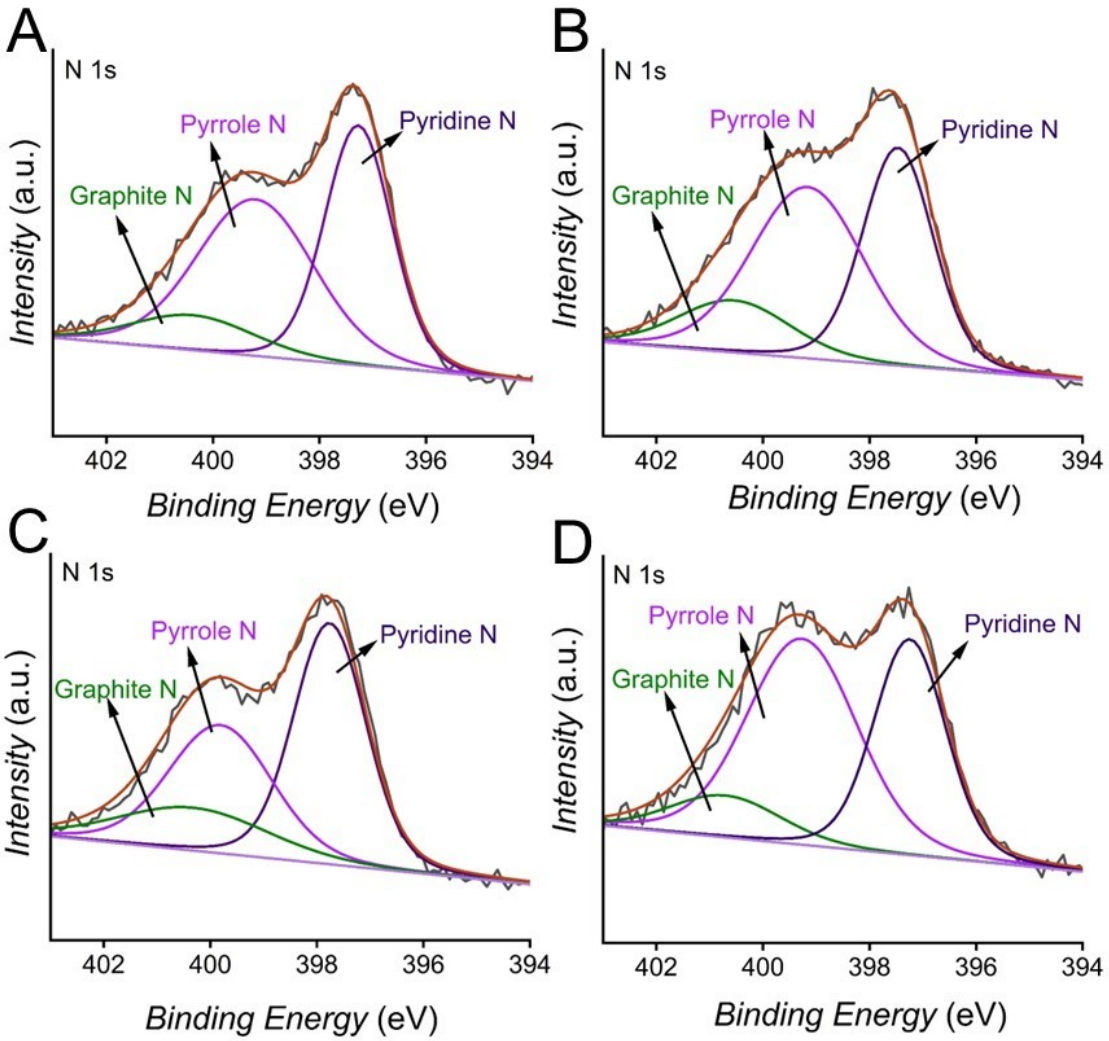

Figure S8: N *1s* XPS data of **(A)** FeMo-NC1, **(B)** FeMo-NC2, **(C)** FeMo-NC3 and **(D)** FeNC; containing nafion on ITO.

For the better understanding of chemical composition in the surface of the samples, the XPS survey was done on the material containinng different elemental content (C, N, Fe, Mo and O). The elemental percentage can be estimated by using following equation.[1,2]

$$At.\% = \frac{A_i / SFi}{\sum A_i / SF_i}$$

Where, i=C/N/Mo/Fe/O; A_i: area under the curves, $SF_C = 0.25$, $SF_N = 0.42$, $SF_{Mo} = 3.32$, $SF_{Fe} = 3$ and $SF_O = 0.66$.

Table S1: Surface Composition of elements using XPS. () indicates surface composition after HER.

Sl. No.	Sample Name	Surface compositions (% at.)				
		O	C	Fe	N	Mo
1	FeMo-NC1	9.95 (11.307)	79.25 (79.06)	5.44 (5.14)	5.16 (4.38)	0.178 (0.113)
2	FeMo-NC2	8.83 (11.33)	78.31 (78.17)	5.15 (4.98)	7.48 (5.502)	0.208 (0.194)
3	FeMo-NC3	10.84 (12.69)	76.78 (76.58)	4.78 (4.42)	7.25 (6.11)	0.336 (0.192)

Table S2: Surface oxidation state of Fe.

Sample Name	Fe	Positions (eV)	Area%	Fe (%) in different oxidation state
FeNC	Fe^0 $2p_{3/2}$	706.52	9.19	14.3
	Fe^0 $2p_{1/2}$	720.19	5.11	
	Fe^{2+} $2p_{3/2}$	709.26	17.45	27.27
	Fe^{2+} $2p_{1/2}$	722.72	9.82	
	Fe^{3+} $2p_{3/2}$	714.63	23.15	34.61
	Fe^{3+} $2p_{1/2}$	727.23	11.46	
	Fe sat.	717.6	15.26	NA
	Fe sat.	733.91	8.56	

Table S3: Surface oxidation state of Fe.

Sample Name	Fe	Positions (eV)	Area%	Fe (%) in different oxidation state
FeMo-NC1	Fe^0 $2p_{3/2}$	706.18	10.91	16.77
	Fe^0 $2p_{1/2}$	720.1	5.86	
	Fe^{2+} $2p_{3/2}$	709.87	19.47	29.2
	Fe^{2+} $2p_{1/2}$	722.35	9.73	
	Fe^{3+} $2p_{3/2}$	714.33	20.7	30.22
	Fe^{3+} $2p_{1/2}$	727.6	9.52	
	Fe sat.	717.26	15.86	NA
	Fe sat.	733.56	7.93	

Table S4; Surface oxidation state of Fe.

Sample Name	Fe	Positions (eV)	Area%	Fe (%) in different oxidation state
FeMo-NC2	Fe^0 $2p_{3/2}$	706.37	11.6	16.72
	Fe^0 $2p_{1/2}$	718.92	5.12	
	Fe^{2+} $2p_{3/2}$	709.7	21.1	32.15
	Fe^{2+} $2p_{1/2}$	722.14	11.05	
	Fe^{3+} $2p_{3/2}$	714.45	20.97	31.07
	Fe^{3+} $2p_{1/2}$	728.2	10.1	
	Fe sat.	717.46	13.36	NA
	Fe sat.	733.97	6.68	

Table S5: Surface oxidation state of Fe.

Sample Name	Fe	Positions (eV)	Area%	Fe (%) in different oxidation state
FeMo-NC3	Fe^{0} $2p_{3/2}$	706.18	13.62	20.57
	Fe^{0} $2p_{1/2}$	720	6.95	
	Fe^{2+} $2p_{3/2}$	709.95	18.96	28.47
	Fe^{2+} $2p_{1/2}$	723.04	9.51	
	Fe^{3+} $2p_{3/2}$	714.21	20.44	30.4
	Fe^{3+} $2p_{1/2}$	728.87	9.96	
	Fe sat.	717.27	13.7	NA
	Fe sat.	734.14	6.85	

Table S6: Surface oxidation state of Mo.

Sample Name	Mo	Positions (eV)	Area%	Mo (%) in different oxidation state
FeMo-NC1	Mo^{4+} $3d_{5/2}$	229.63	25.24	40.61
	Mo^{4+} $3d_{3/2}$	232.54	15.37	
	Mo^{6+} $3d_{5/2}$	231.27	35.73	59.38
	Mo^{6+} $3d_{3/2}$	233.76	23.65	

Table S7: Surface oxidation state of Mo.

Sample Name	Mo	Positions (eV)	Area%	Mo (%) in different oxidation
FeMo-NC2	Mo^{4+} $3d_{5/2}$	229.87	16.4	27.5
	Mo^{4+} $3d_{3/2}$	232.62	11.11	
	Mo^{6+} $3d_{5/2}$	231.44	40.39	72.49
	Mo^{6+} $3d_{3/2}$	234.18	32.1	

Table S8: Surface oxidation state of Mo.

Sample Name	Mo	Positions (eV)	Area%	Mo (%) in different
FeMo-NC3	Mo^{4+} $3d_{5/2}$	230.25	20.3	33.52
	Mo^{4+} $3d_{3/2}$	232.78	13.22	
	Mo^{6+} $3d_{5/2}$	231.5	40.27	69.76
	Mo^{6+} $3d_{3/2}$	234.53	26.49	

ICP-MS

First, we prepare a solution of standard known samples with different concentrations, and we get a linear plot as shown in graph. From that graph we get the slope and intercept, and we can use it to calculate the concentration of unknown solution contain Mo.

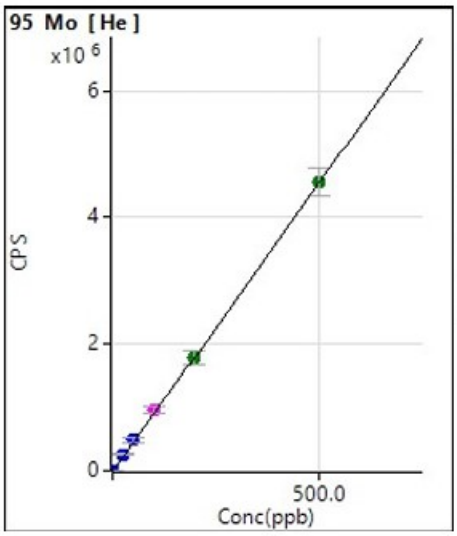

	Rjct	Conc.	Calc Conc.	CPS	Ratio	Det.	RSD	%RE
1	☐	0.000	0.000	2700.37		P	18.8	
2	☐	25.000	26.985	248840.84		P	12.0	7.9
3	☐	50.000	52.499	481567.32		P	14.6	5.0
4	☐	100.000	105.843	968140.56		M	12.7	5.8
5	☐	200.000	196.598	1795949.29		A	12.1	-1.7
6	☐	500.000	499.843	4561971.08		A	10.1	0.0

y = 9121.4054 * x + 2700.3700
R = 0.9999
DL = 0.1673 ppb
BEC = 0.296 ppb
Weight: <None>
Min Conc: 0

Figure S9: Linear fit of known standard solution of Mo.

The ICP-MS gives us Mo = 4.594 ppb in the FeMo-NC1.
We have the diluation factor of 20/0.1 =200 times in the sample.
The real concentration of the digestion solution is = 4.594 x 200 = 918.8 ppb = 0.9188 ppm (mg/L)
We know that all the Mo came from the solid sample and is contained in 50 mL.
Total amount of Mo in 50 mL = 0.9188 x 50/1000 = 0.04594 mg
So, 5 mg of FeMoNC2 contains 0.04595 mg of Mo.

In this way we can calculate and get 0.06067 mg and 0.15484 mg amount of Mo in FeMo-NC2 and FeMo-NC3 respectively in 5 mg of sample each sample.

As we know the sample yield so we can verify the theoretical mass% Mo with experimental mass% Mo.

Table S9: Comparison of Theroticial and experimental content of Mo in FeMo-NC1, FeMo-NC2 and FeMo-NC3 from ICP-MS.

Sl. No.	Sample Name	Theoritical Mass %Mo	Experimental Mass %Mo
1	FeMo-NC1	0.94	0.91
2	FeMo-NC2	1.25	1.21
3	FeMo-NC3	3.18	3.08

Table S10: ICP-MS data before and after catalysis.

FeMo-NC2	Fe (mg)	Mo (mg)
Before Catalysis	0.32953	0.06067
After Catalysis	0.31477	0.05907

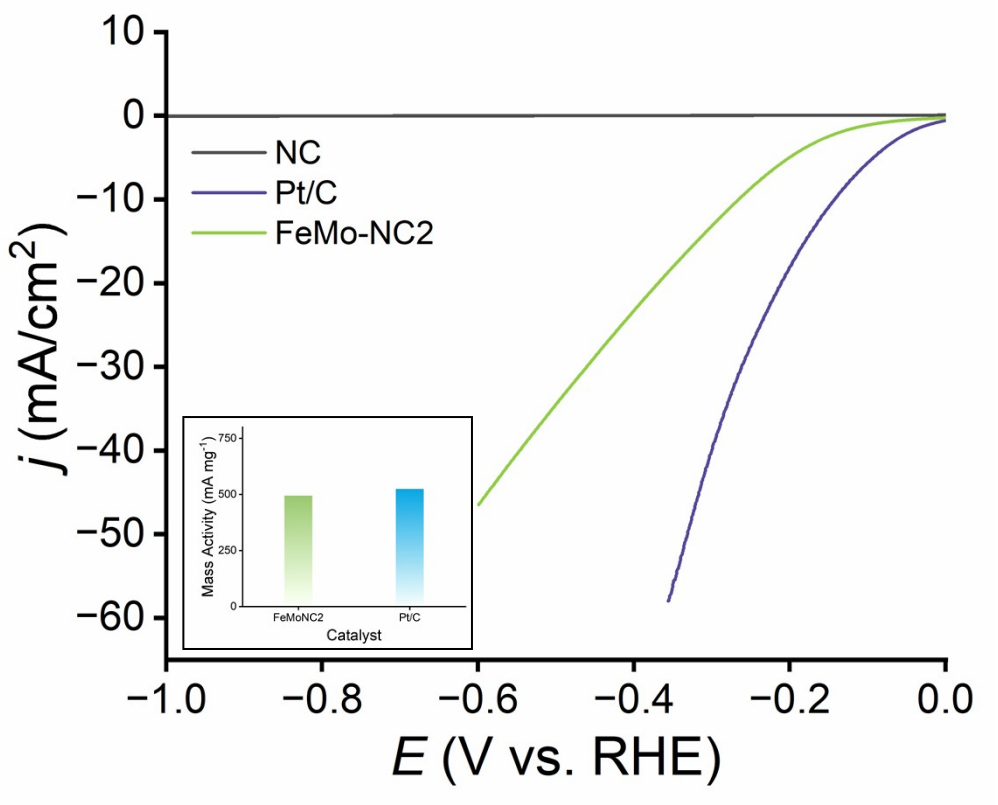

Figure S10: LSVs recorded at scan rate 20 mV/s on ITO in 0.1 M KOH. Inset represents mass activity of FeMoNC2 and Pt/C.

Table S11: EIS circuit fitted data for the sample.

Sample Name	Rs (Ω)	CPE ($\mu F. s^{(n-1)}$)	Rct (Ω)	R_{pore} (Ω)
FeMo-NC1	165.2	11.94	4843	1650
FeMo-NC2	185.7	23.51	1821	313.8
FeMo-NC3	168.7	12.19	3836	14101

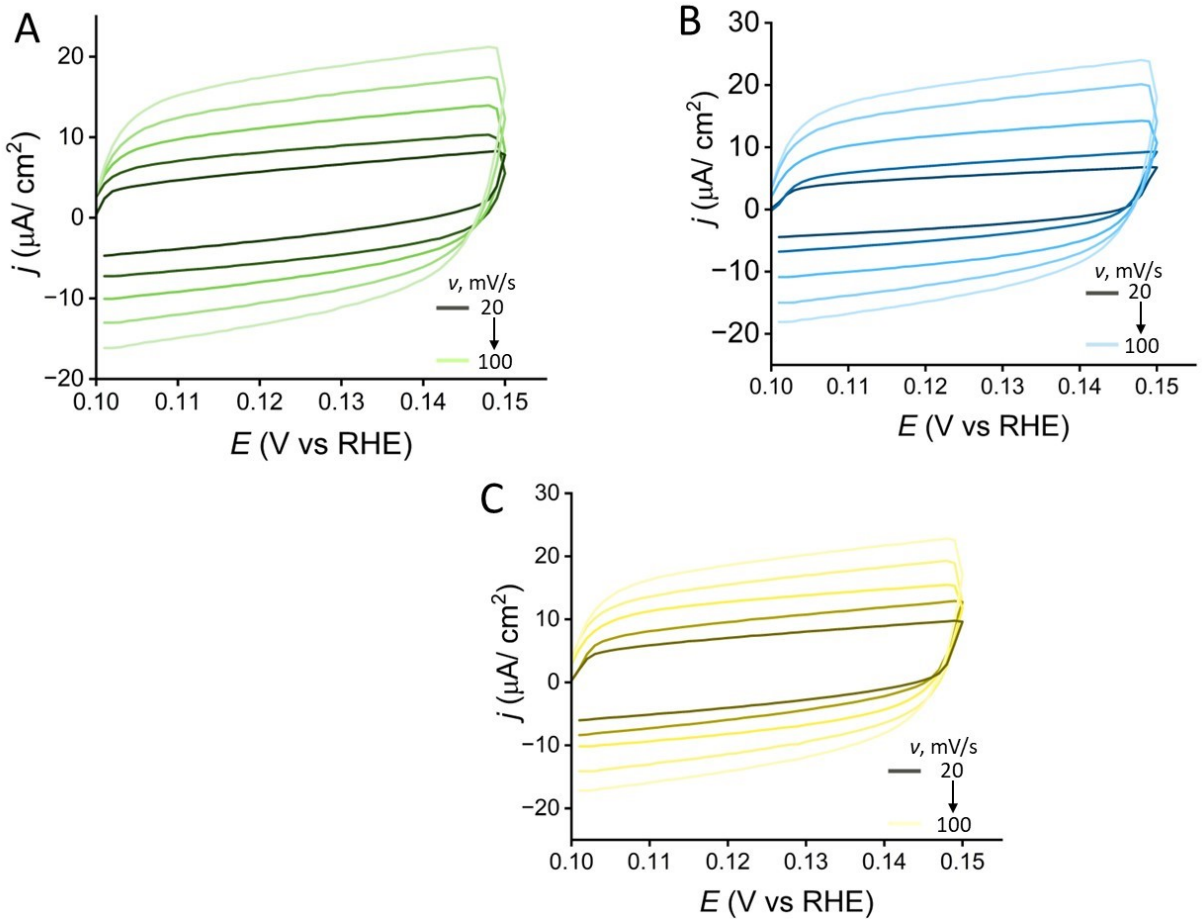

Figure S11: CV at different scan rate for C_{dl} measurement of (A) FeMo-NC1, (B) FeMo-NC2, (C) FeMo-NC3; on ITO, Solution 0.1 M KOH.

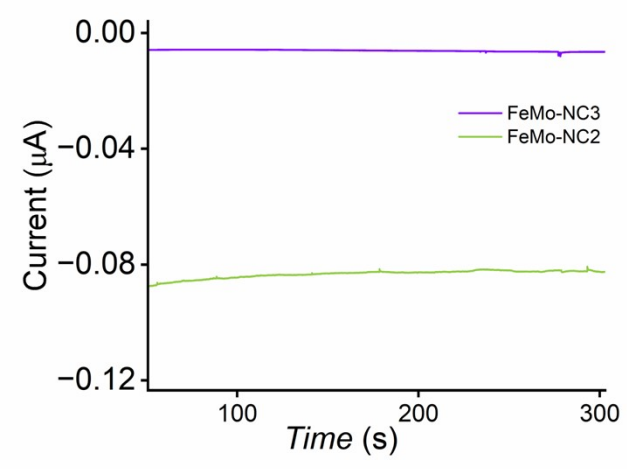

Figure S12: i-*t* curves on coated ultramicroelectrode for FeMoNC2 and FeMoNC3.

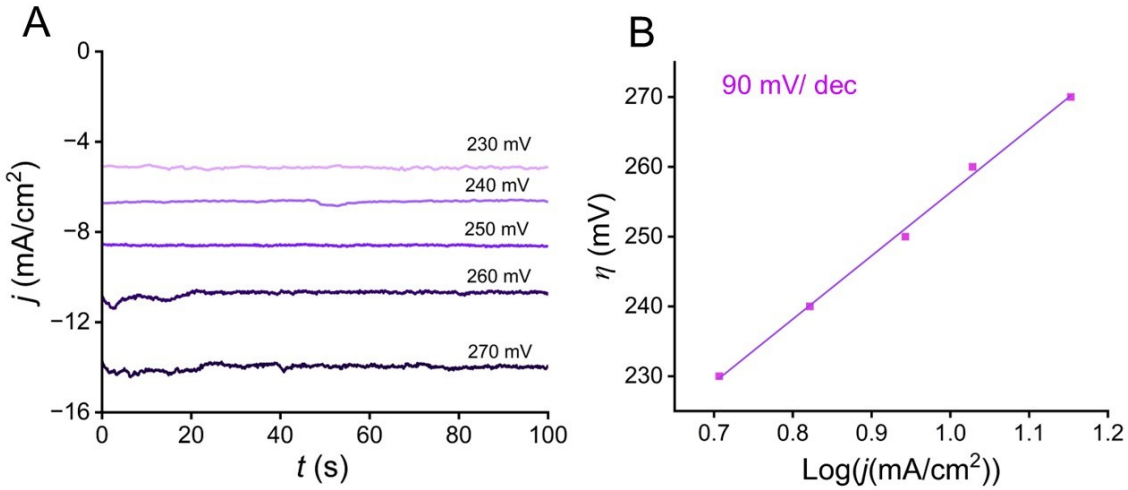

Figure S13: (A) i-*t* curves at different overpotential, and **(B)** Tafel plot of FeMo-NC2, on ITO in 0.1 M KOH.

Density Functional Theory (DFT) Calculations

First-principles calculations were performed using the plane-wave pseudopotential method as implemented in the Quantum ESPRESSO package.[3,4] The exchange-correlation interaction was described by the Generalized Gradient Approximation (GGA) with the Perdew-Burke-Ernzerhof (PBE) functional.[5] Ultrasoft pseudopotentials (USPP) were employed to describe the electron-ion interactions for all atomic species.[6] The kinetic energy cutoff for wavefunctions and charge density was set to ensure convergence of total energies to within 10^{-5} eV/atom.

The bulk Fe_2C structure was adopted from the Materials Project database (Space Group: P6/mmm, No. 191) with optimized lattice parameters of a = b = 3.699 Å and c = 2.642 Å.[7] To model the catalytic surface, a 3×3 supercell of the 001 slab of Fe_2C slab was constructed. This slab was interfaced with a graphitic nitrogen-doped graphene (NG) sheet, the structure of which was adapted from the work of Banerjee et al.[8] To investigate the effect of molybdenum doping, a single Fe atom in the surface layer was substituted with a Mo atom.

Geometry Optimization and Electronic Structure

The d-band center (ε_d) was computed according to the **Nørskov d-band model** , defined as the first moment of the projected d-states relative to the Fermi level (E_F):

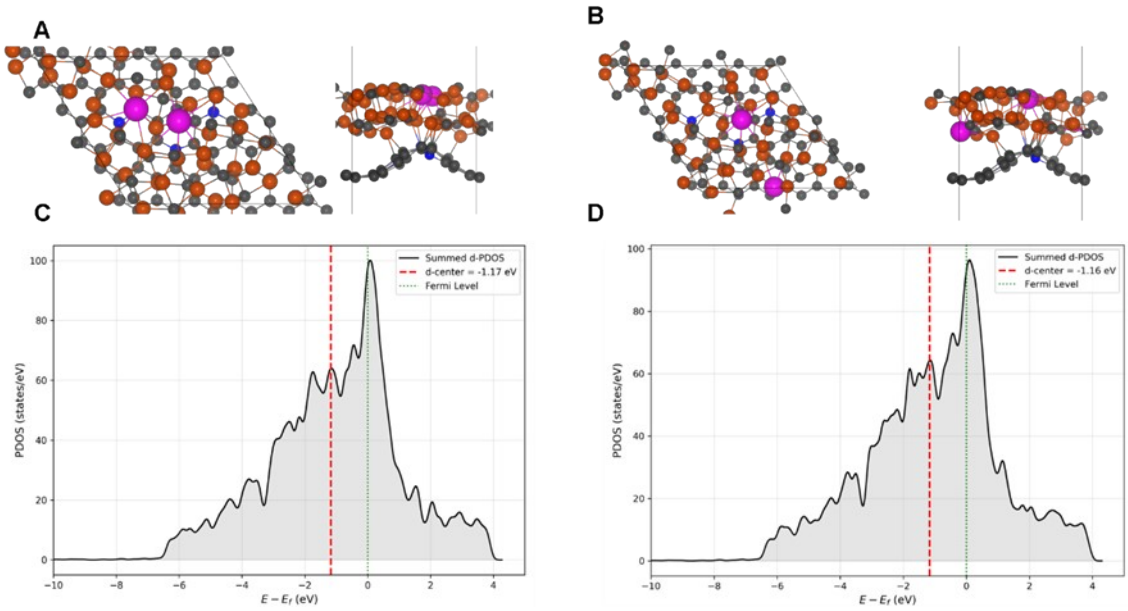

Figure S14: Optimized geometric structures of the catalytic systems. (A) Top and side views of the 2Mo-Fe2C/NG (proximal) heterostructure. (B) Top and side views of the 2Mo-Fe2C/NG (distal) heterostructure. The atoms are identified by color: Iron (orange), Carbon (grey), Nitrogen (blue), and Molybdenum (magenta). Calculated projected density of states (PDOS) for the d-orbitals of the active metal sites. (C) The summed Fe d-PDOS for the 2Mo-Fe2C/NG (proximal) surface, (D) The summed d-PDOS for thesssss 2Mo-Fe2C/NG (distal) surface The Fermi level is set to 0 eV (green dotted line). Partial Density of States (PDOS) illustrating the orbital hybridization between the surface-active sites and the adsorbed oxygen species.

$$\varepsilon_d = \frac{\int_{-\infty}^{\infty} (E - E_F) \cdot \rho_d(E)\ dE}{\int_{-\infty}^{\infty} \rho_d(E)\ dE}$$

where ρ_d represents the density of states projected onto the d-orbitals of the active metal sites.[9,10]

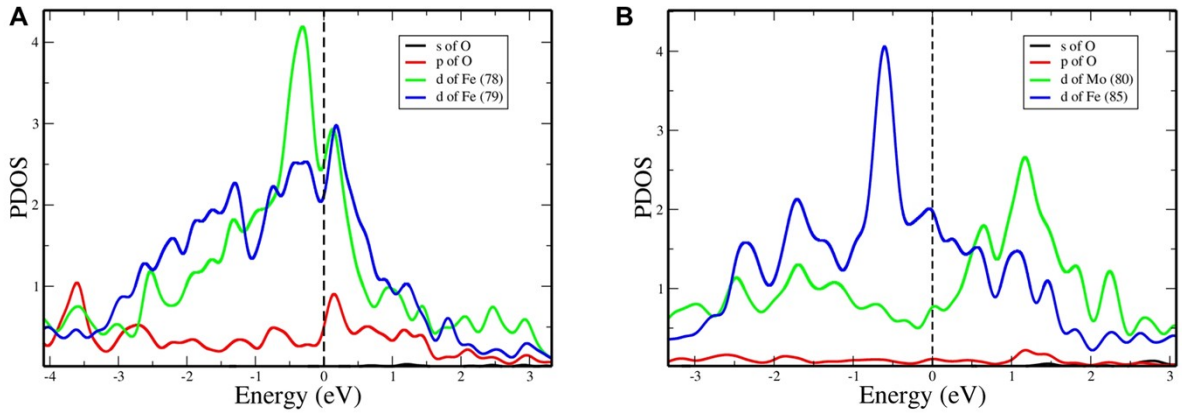

Figure S15. Partial Density of States (PDOS) illustrating the orbital hybridization between the surface active sites and the adsorbed oxygen species. **(A)** Pure Fe_2C/NG surface, showing strong, sharp overlap between O *2p* (red) and Fe *3d* (green/blue) orbitals, indicative of strong binding. **(B)** Mo-Fe_2C/NG surface, displaying modified hybridization between O *2p*, Mo *4d* (green), and Fe *3d* (blue) orbitals, corresponding to optimized binding strength.

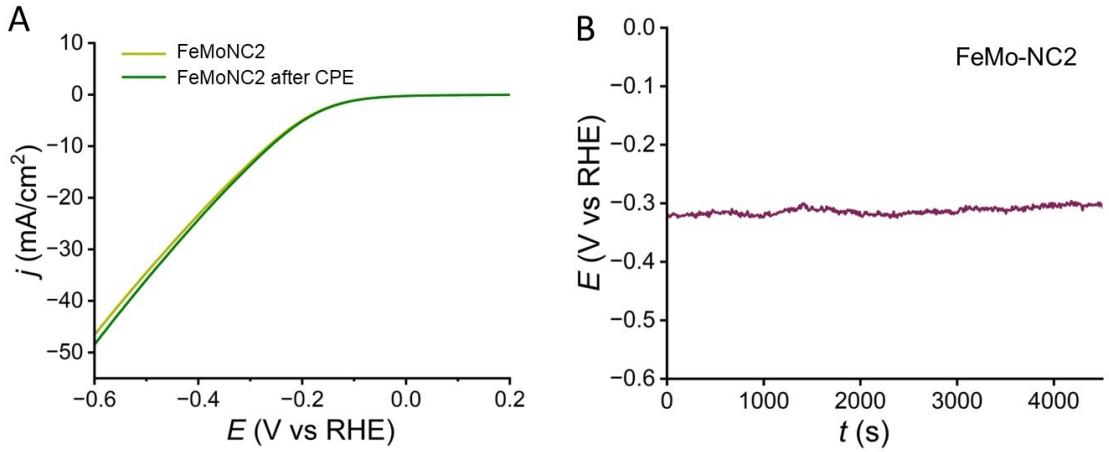

Figure S16: (A) LSV before and after electrocatalysis, and **(B)** chronopotentiometry of FeMo-NC2 on ITO in 0.1 M KOH.

Post-HER

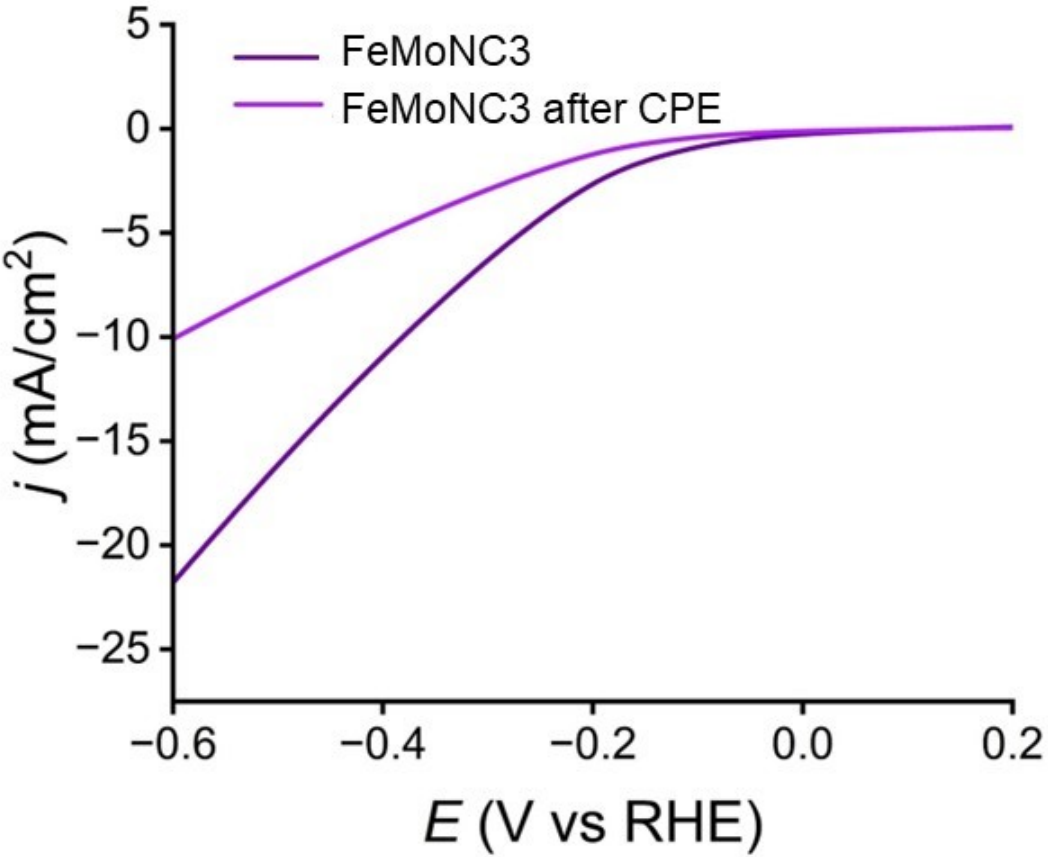

Figure S17: LSV of FeMo-NC3 before and after electrocatalysis on ITO in 0.1 M KOH.

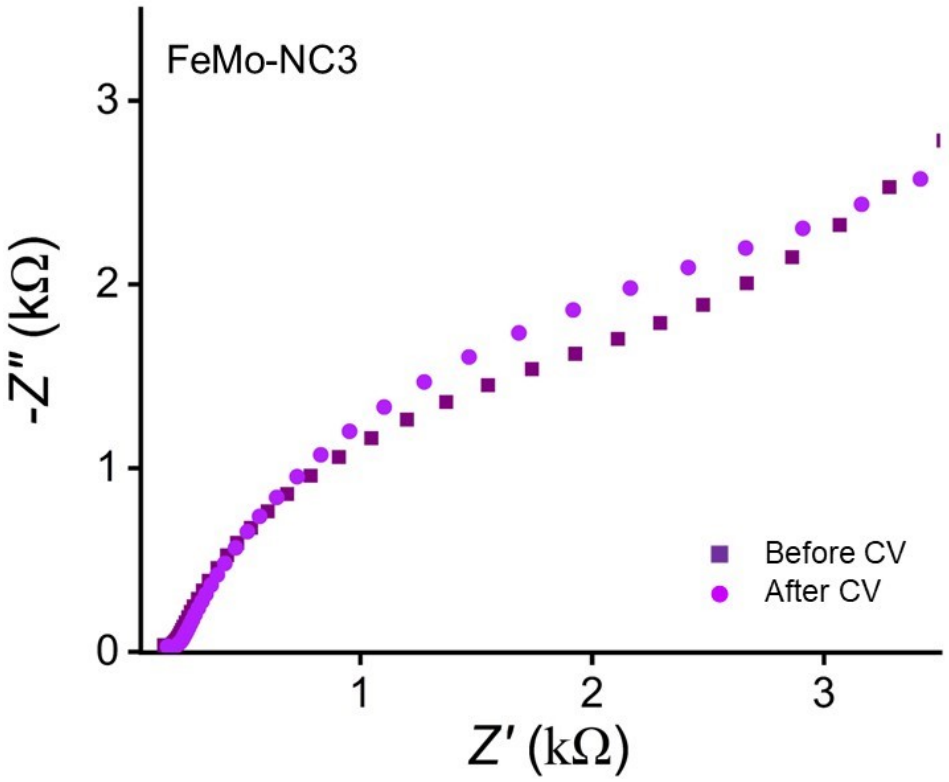

Figure S18: EIS before and after electrocatalysis for FeMo-NC3 in 0.1 M KOH on ITO.

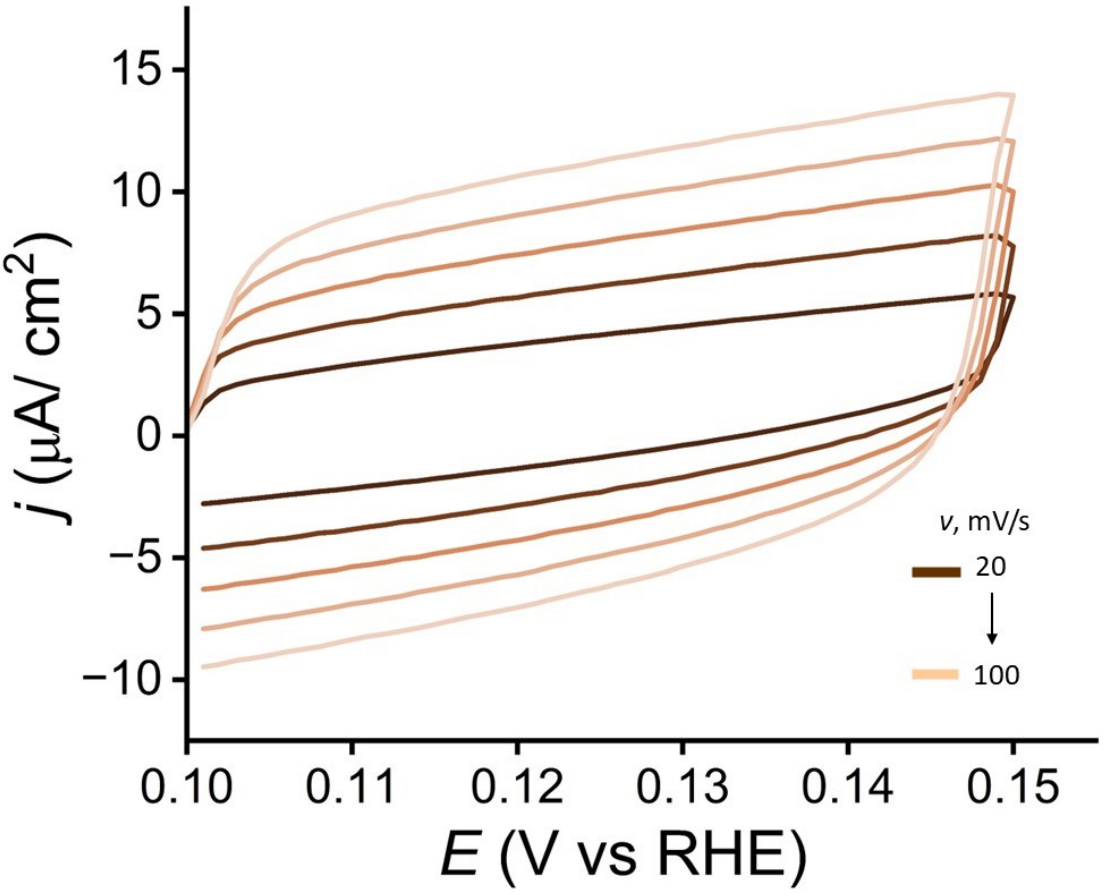

Figure S19: CV at different scan rates of FeMo-NC3 after electrocatalysis on ITO in 0.1 M KOH.

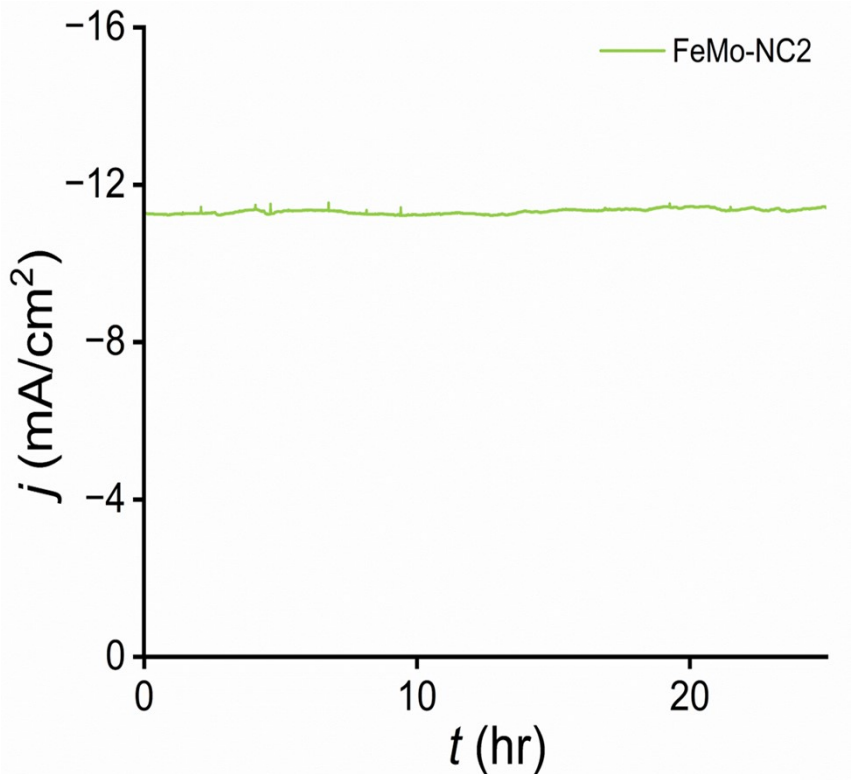

Figure S20: *i-t* response for FeMo-NC2 on ITO in 0.1M KOH.

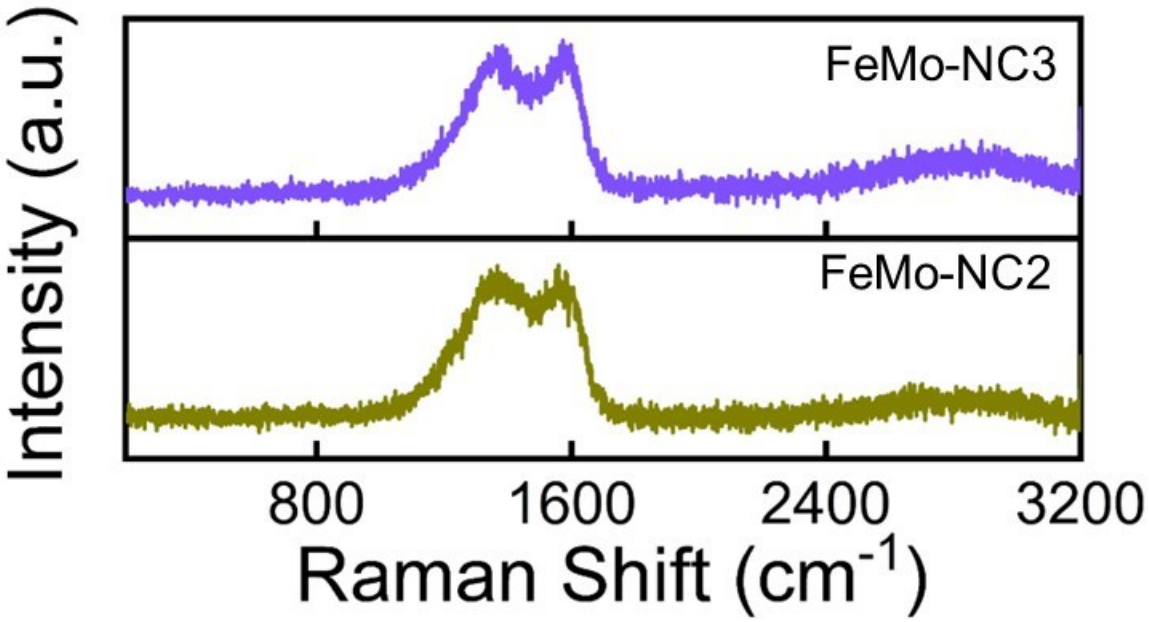

Figure S21: After electrocatalysis Raman spectra of FeNC2 and FeNC3.

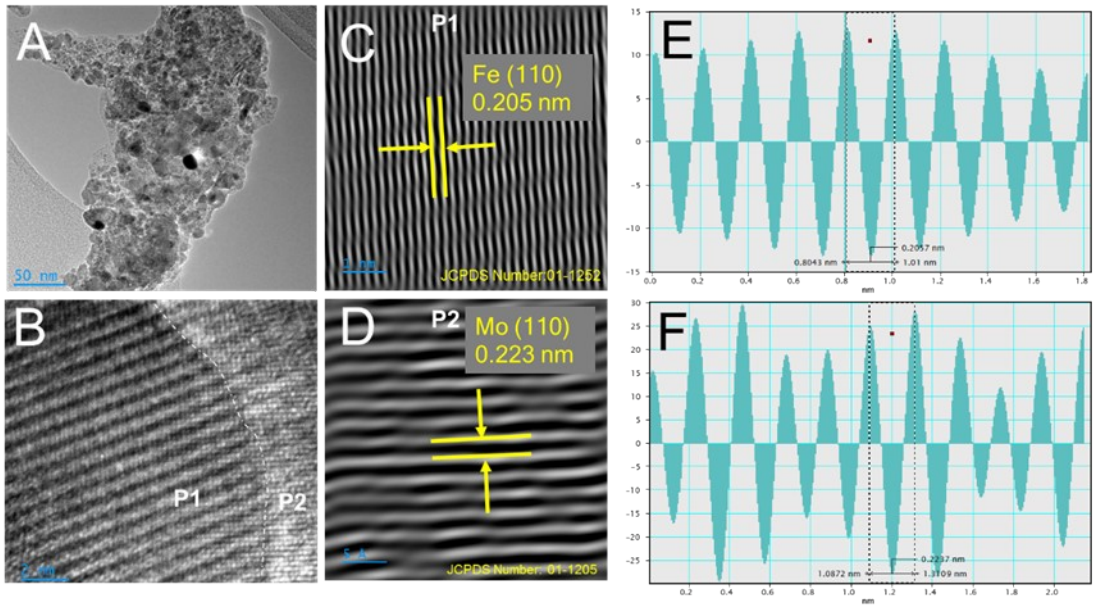

Figure S22: (A) Post-HER TEM, **(B)** HRTEM, **(C, D)** IFFT pattern of the P1 and P2 region, **(E, F)** corresponding line spectrum of FeMo-NC2.

Table S12: Comparison table of Transition metal -C based electrocatalysts for hydrogen evolution with FeMo-NC2.

Catalyst	Electrolyte	Substate	ECSA normalized Activity	Catalyst Loading (mg cm^{-2})	Overpotential (mV)	Tafel Slope (mV/dec)	Durability	Ref.
BC-Mo/Co	1.0 M KOH	GCE	0.004	0.15	257	51	NA	[11]
FeMn@BNPCFs-800	1.0 M KOH	GCE	-	0.306	311	127.69	NA	[12]
Mo2C NC@Fe/Fe3C	1.0 M KOH	GCE	-	0.28	252	110	16 hrs	[13]
Mo/Mo2C/N-CNFs	1.0 M PBS	GCE	0.122	1.68	294	130.6	2000 cycles	[14]
2Co-NC-700	1.0 M KOH	GCE	0.00018	0.955	303	178.2	24 hrs	[15]
Co/W-C@NC NSs(600)	1.0 M KOH	GCE	0.016	0.024	418	167	10 hrs	[16]
Ni@NCS-800	1.0 M KOH	Ni foam	4.58	0.05	330	32	4 hrs	[17]
Mo_2C	1.0 M KOH	On FTO	-	-	270	78	10 hrs	[18]
FeMo/Mo_2C@C	-	Carbon paper	-	0.0375	219	36.8	18 hrs	[19]
Ti_3C_2-CoS_2	1.0 M KOH	Ni foam	-	0.3	276	159	10 hrs	[20]
Fe@C-SN/50	1.0 M KOH	GCE	0.01	0.55	550	358	-	[21]
MoO_3/AC	1.0 M KOH	Stainless steel	0.065	-	353	124	15 hrs	[22]
FeMo-NC2	**0.1 M KOH**	**On ITO**	**2.35**	**1**	**260**	**90**	**25 hrs**	**TW**

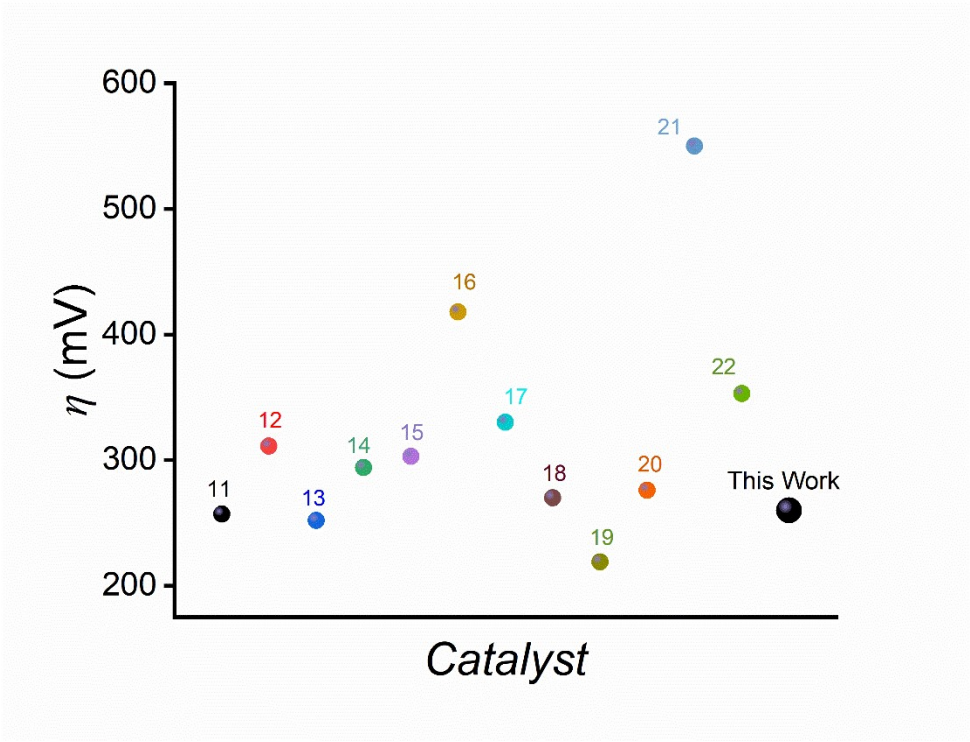

Figure S23: Position of this work in comparison to recent published work.

References

1 R. Nandan, P. Pandey, A. Gautam, O. Y. Bisen, K. Chattopadhyay, M.-M. Titirici and K. K. Nanda, *ACS Appl. Mater. Interfaces*, 2021, **13**, 3771–3781.

2 S. Kumar, R. Kumar, N. Goyal, A. Vazhayil, A. Yadav, N. Thomas and B. Sahoo, *ACS Appl. Nano Mater.*, 2024, **7**, 7865–7882.

3 P. Giannozzi, S. Baroni, N. Bonini, M. Calandra, R. Car, C. Cavazzoni, D. Ceresoli, G. L. Chiarotti, M. Cococcioni and I. Dabo, *Journal of physics: Condensed matter*, 2009, **21**, 395502.

4 P. Giannozzi, O. Andreussi, T. Brumme, O. Bunau, M. Buongiorno Nardelli, M. Calandra, R. Car, C. Cavazzoni, D. Ceresoli and M. Cococcioni, *Journal of physics: Condensed matter*, 2017, **29**, 465901.

5 J. P. Perdew, K. Burke and M. Ernzerhof, *Phys. Rev. Lett.*, 1996, **77**, 3865.

6 D. Vanderbilt, *Phys. Rev. B*, 1990, **41**, 7892.

7 A. Jain, S. P. Ong, G. Hautier, W. Chen, W. D. Richards, S. Dacek, S. Cholia, D. Gunter, D. Skinner and G. Ceder, *APL Mater.*

8 A. Banerjee, S. Jain, S. G. Dastider, R. Biswas, S. Das, K. Mondal, V. Vishal, G. K. Lahiri and A. Dutta, *Small*, 2025, **21**, 2406765.

9 B. Hammer and J. K. Nørskov, in *Advances in catalysis*, Elsevier, 2000, vol. 45, pp. 71–129.

10 B. Hammer and J. K. Nørskov, *Surf. Sci.*, 1995, **343**, 211–220.

11 J. Ñanculeo, T. Andreu, I. Sirés, A. Ramírez, M. Cea, B. Nahuelcura, G. Valenzuela, K. Garrido-Miranda and M. E. González, *Biochar*, 2025, **7**, 72.

12 Z. Liu, F. Guo, L. Han, J. Xiao, X. Zeng, C. Zhang, P. Dong, M. Li and Y. Zhang, *ACS Appl. Mater. Interfaces*, 2022, **14**, 13280–13294.

13 S. Wang, G. Bendt, S. Saddeler and S. Schulz, *Energy Technology*, 2019, **7**, 1801121.

14 M. Li, H. Wang, Y. Zhu, D. Tian, C. Wang and X. Lu, *Appl. Surf. Sci.*, 2019, **496**, 143672.

15 J. Lv, P. Hu, J. Zheng, S. Mo, W. Liu, S. Chen and Y. Liu, *J. Power Sources*, 2024, **602**, 234339.

16 T. Zhao, J. Gao, J. Wu, P. He, Y. Li and J. Yao, *Energy Technology*, 2019, **7**, 1800969.

17 K. B. Patel, B. Parmar, K. Ravi, R. Patidar, J. C. Chaudhari, D. N. Srivastava and G. R. Bhadu, *Appl. Surf. Sci.*, 2023, **616**, 156499.

18 C. G. Morales-Guio, K. Thorwarth, B. Niesen, L. Liardet, J. Patscheider, C. Ballif and X. Hu, *J. Am. Chem. Soc.*, 2015, **137**, 7035–7038.

19 H. Li, T. Wang, M. Xu, P. Wang, Z. Gao, W. Zhang, M. Liu and M. Feng, *J. Alloys Compd.*, 2024, **987**, 174199.

20 S. B. Devi and R. Navamathavan, *J. Electrochem. Soc.*, 2023, **170**, 096503.

21 A. Jaiswal, R. Kumar and R. Prakash, *Energy & Fuels*, 2021, **35**, 16046–16053.

22 S. Sekar, J.-S. Yun, S. Park, D. Y. Kim, Y. Lee and S. Lee, *Int. J. Energy Res.*, 2024, **2024**, 3167699.